

PREDICTION OF THE PROTON-TO-TOTAL TURBULENT HEATING IN THE SOLAR WIND

G. G. HOWES

Department of Physics and Astronomy, University of Iowa, Iowa City, IA, 52242
Draft version November 23, 2018

ABSTRACT

This paper employs a recent turbulent heating prescription to predict the ratio of proton-to-total heating due to the kinetic dissipation of Alfvénic turbulence as a function of heliocentric distance. Comparing to a recent empirical estimate for this turbulent heating ratio in the high-speed solar wind, the prediction shows good agreement with the empirical estimate for $R \gtrsim 0.8$ AU, but predicts less ion heating than the empirical estimate at smaller heliocentric radii. At these smaller radii, the turbulent heating prescription, calculated in the gyrokinetic limit, fails because the turbulent cascade is predicted to reach the proton cyclotron frequency before Landau damping terminates the cascade. These findings suggest that the turbulent cascade can reach the proton cyclotron frequency at $R \lesssim 0.8$ AU, leading to a higher level of proton heating than predicted by the turbulent heating prescription in the gyrokinetic limit. At larger heliocentric radii, $R \gtrsim 0.8$ AU, this turbulent heating prescription contains all of the necessary physical mechanisms needed to reproduce the empirically estimated proton-to-total heating ratio.

Subject headings: turbulence — solar wind

1. INTRODUCTION

In the development of a thermodynamic model of the heliosphere, a crucial issue is the identification of the various physical mechanisms that play a role in determining the temperature profiles of the heliospheric plasma ions and electrons. Some of the effects influencing the measured temperature profiles in the inner heliosphere are energy conservation in the spherically expanding plasma, heat conduction, Coulomb collisions, and plasma heating through the dissipation of solar wind turbulence.¹ The incorporation of the first three of these effects is relatively well understood, but the heating of the heliospheric ions and electrons resulting from the dissipation of solar wind turbulence remains an area of active research.

Although a number of studies have addressed the issue of plasma heating by the dissipation of turbulence (see Cranmer et al. (2009) for a review of previous efforts), with the exception of a pioneering series of papers by Quataert and Gruzinov (Quataert 1998; Gruzinov 1998; Quataert & Gruzinov 1999), the turbulent heating of the ions and electrons separately has only recently become a focus of interest. We review here three studies that have made progress in the investigation of turbulent plasma heating and the effect of this heating on the solar wind proton and electron temperature profiles.

Breech et al. (2009) coupled an existing turbulence transport model for the solar wind (Zank et al. 1996; Matthaeus et al. 1999; Smith et al. 2001; Breech et al. 2008) to separate radial evolution equations for the proton and electron temperatures. The temperature equations included the effects of spherical expansion, parallel electron heat flux, collisional energy exchange between protons and electrons, and separate turbulent heating rates for the ions and electrons. The kinetic dissipation mechanisms that determine the partitioning of tur-

bulent heating between protons and electrons were not addressed in this model, so the fraction of proton-to-total turbulent heating was set to a constant value, $f_p = Q_p/(Q_p + Q_e)$. The model achieved a reasonable accounting for the temperature data measured by *Ulysses* when the effect of Coulomb collisions was weak, the electron heat conduction was provided by an empirically determined function, and the partitioning of turbulent heating was taken as $f_p = 0.6$. Note that the value of $f_p = 0.6$ is consistent with other estimates of the fraction of proton heating (Leamon et al. 1999; Stawarz et al. 2009).

In a complementary work, Cranmer et al. (2009) constructed a model following the internal energy evolution of the protons and electrons in the solar wind in an attempt to constrain empirically the required proton and electron turbulent heating in the solar wind. Assuming isotropic Maxwellian proton and electron velocity distributions with shared bulk velocity, separate equations for the conservation of energy in a spherically expanding flow for protons and electrons were constructed to incorporate the effects of energy exchange by Coulomb collisions, parallel electron heat conduction, and turbulent heating of protons and electrons. Using analytic fits to *Helios* and *Ulysses* measurements for the proton temperature, electron temperature, and parallel electron heat conduction flux, the equations were solved for the turbulent proton and electron heating rates. The results were then combined to obtain an empirical estimate of the proton-to-total heating rate $Q_p/(Q_p + Q_e)$ as a function of heliocentric radius, reproduced as the dashed line in Figure 1.

Based on a theoretical model of the turbulent cascade of energy in a weakly collisional plasma (Howes et al. 2008a), Howes (2010) predicted the proton-to-electron heating ratio Q_p/Q_e resulting from the dissipation of Alfvénic turbulence. The key result of this study was an analytical prescription for the heating ratio $Q_p/Q_e(\beta_p, T_p/T_e)$, a function of only two plasma pa-

¹ Pickup ions are believed to significantly affect the heliospheric energy balance only in the outer heliosphere at $R \gtrsim 10$ AU (Breech et al. 2009).

rameters, the proton plasma beta β_p and the proton-to-electron temperature ratio T_p/T_e . The limits of validity of this heating ratio prediction were given as a constraint on the minimum scale of turbulent energy injection (assuming an isotropic driving mechanism for the turbulence).

This paper describes the application of the Howes (2010) heating prescription to predict the proton-to-total turbulent heating rate $Q_p/(Q_p + Q_e)$ for the high-speed solar wind and compares the resulting prediction to the empirical estimate of Cranmer et al. (2009).

2. PREDICTION OF TURBULENT HEATING

This section describes the prediction of the ratio of the proton-to-total turbulent heating $Q_p/(Q_p + Q_e)$ in the high-speed solar wind as a function of heliocentric radius R using the turbulent heating prescription by Howes (2010). Since this prescription depends on the plasma parameters β_p and T_p/T_e , it is necessary to construct a model of the high-speed solar wind to determine the variation of these plasma parameters with heliocentric radius. In §2.1, we describe the solar wind model. In §2.2, we review the theoretical framework of low-frequency, anisotropic Alfvénic turbulence in a magnetized, weakly collisional plasma that underlies the turbulent heating prescription. This prescription is employed to predict the proton-to-total turbulent heating $Q_p/(Q_p + Q_e)$ in §2.3. In §2.4, we estimate the evolution of the width of the inertial range in the high-speed solar wind in order to verify the validity of the turbulent heating prescription in §2.5.

2.1. Solar Wind Model

We adopt the same specific model for the high-speed solar wind used by Cranmer et al. (2009) to facilitate the comparison to their empirical turbulent heating estimate. This model is used to specify, as a function of heliocentric radius R , the two key plasma parameters required by the turbulent heating prescription: the proton plasma beta β_p and the proton-to-electron temperature ratio T_p/T_e .

Analytic fits to *in situ* measurements of the high-speed solar wind (faster than 600 km s⁻¹) from the *Helios* and *Ulysses* spacecraft over the range 0.29 AU < R < 5.4 AU were used by Cranmer et al. (2009) to generate equations for the proton and electron temperatures as function of heliocentric radius R ,

$$\ln\left(\frac{T_p}{10^5 \text{ K}}\right) = 0.9711 - 0.7988x + 0.07062x^2 \quad (1)$$

$$\ln\left(\frac{T_e}{10^5 \text{ K}}\right) = 0.03460 - 0.4333x + 0.08383x^2, \quad (2)$$

where $x \equiv \ln(R/1 \text{ AU})$.

In addition to the proton temperature, we need to specify the form of the proton density and magnetic field strength to determine the proton plasma beta $\beta_p = 8\pi n_p T_p / B^2$. Following Cranmer et al. (2009), we take a proton density of the form

$$n_p(R) = n_0(R/1 \text{ AU})^{-2} \quad (3)$$

where $n_0 = 2.5 \text{ cm}^{-3}$. The empirical turbulent heating constraints calculated by Cranmer et al. (2009) used a

colatitude $\theta = 15^\circ$ to model the high-latitude *Ulysses* measurements. For the heliocentric distances covered by this model, the winding of the magnetic field into the Parker spiral for the high-speed streams at this colatitude is relatively weak, so a simple monopolar model for the magnetic field strength is a reasonable approximation,

$$B(R) = B_0(R/1 \text{ AU})^{-2}, \quad (4)$$

with $B_0 = 2.5 \times 10^{-5} \text{ G}$.

Using these functions for T_p , T_e , n_p , and B in high-speed solar wind streams, we find that the proton plasma beta varies from $\beta_p = 0.92$ at 0.29 AU to $\beta_p = 34$ at 5.4 AU, and the proton-to-electron temperature ratio varies from $T_p/T_e = 3.9$ at 0.29 AU to $T_p/T_e = 1.3$ at 5.4 AU.

2.2. Turbulent Cascade Model

The heating prescription presented in Howes (2010) is determined using a model for the turbulent cascade of energy in a magnetized, weakly collisional plasma (Howes et al. 2008a). The cascade model determines the steady state form of the magnetic energy spectrum of Alfvénic fluctuations, based on three primary assumptions: (1) the Kolmogorov hypothesis that the energy cascade is determined by local interactions (Kolmogorov 1941); (2) the turbulence maintains a state of critical balance at all scales (Goldreich & Sridhar 1995); and (3) the linear kinetic damping rates are applicable in the nonlinearly turbulent plasma.

The dependence of the nonlinear energy transfer rate on the local turbulent fluctuations in the cascade model (Howes et al. 2008a) is inspired by the following theoretical picture of low-frequency, anisotropic Alfvénic turbulence in a magnetized, weakly collisional plasma (Howes 2008; Schekochihin et al. 2009). The energy of Alfvénic fluctuations is injected into the turbulence isotropically at a scale much larger than the ion Larmor radius, $L_0 \gg \rho_i$, corresponding to an isotropic driving wavenumber $k_0 \rho_i \ll 1$. Since the damping of Alfvénic fluctuations at this large scale by wave-particle interactions in a weakly collisional plasma is negligible, the turbulent fluctuations rise to sufficient amplitudes that nonlinear interactions between counter-propagating Alfvén wave packets transfer the turbulent fluctuation energy to smaller scales. This sets up a critically-balanced, anisotropic cascade of MHD Alfvén waves over all scales down to the perpendicular scale of the ion Larmor radius, $k_\perp \rho_i \lesssim 1$ (Goldreich & Sridhar 1995; Boldyrev 2005)². Even in a weakly collisional plasma, the dynamics of this Alfvén wave cascade is rigorously described by the equations of reduced MHD (Schekochihin et al. 2009). At the perpendicular scale of the ion Larmor radius $k_\perp \rho_i \sim 1$, the turbulence transitions to a critically balanced, anisotropic cascade of kinetic Alfvén waves over the perpendicular scales $k_\perp \rho_i \gtrsim 1$.

The range of scales traversed by the MHD Alfvén wave cascade, between the driving scale and the ion Larmor radius scale, is commonly designated the “inertial range” (Kolmogorov 1941) of MHD turbulence—*i.e.*, the range of scales over which the effects of driving and dissipation are negligible. For a sufficiently

² Perpendicular and parallel are defined with respect to the direction of the local mean magnetic field.

large inertial range, the anisotropy of the energy cascade ($k_{\parallel} \propto k_{\perp}^{2/3}$ in the Goldreich-Sridhar theory, or $k_{\parallel} \propto k_{\perp}^{1/2}$ in the Boldyrev theory) leads to turbulent fluctuations, at the transition to the kinetic Alfvén wave cascade at $k_{\perp}\rho_i \sim 1$, that are highly elongated along the direction of the local magnetic field, $k_{\parallel}/k_{\perp} \ll 1$. Such anisotropic fluctuations are optimally described by a low-frequency expansion of kinetic theory called gyrokinetics (Rutherford & Frieman 1968; Frieman & Chen 1982; Howes et al. 2006; Schekochihin et al. 2009). For Alfvénic fluctuations, the anisotropy implies that, even at scales $k_{\perp}\rho_i \sim 1$, the turbulent fluctuation frequency remains much smaller than the ion cyclotron frequency, $\omega \ll \Omega_i$. This is an important limit for the applicability of gyrokinetic theory, and enables one to determine quantitatively the limit of validity of the heating prescription (see §2.5). When this limit is satisfied, the ion cyclotron resonance plays a negligible role in the collisionless damping of the turbulent fluctuations (Lehe et al. 2009). Instead, collisionless damping of the fluctuations occurs via the both the ion and electron Landau resonances at scales $k_{\perp}\rho_i \gtrsim 1$, implying that the kinetic Alfvén wave cascade comprises the “dissipation range” of Alfvénic turbulence.

It is in the dissipation range that wave-particle interactions transfer the electromagnetic fluctuation energy to the ion and electron particle distribution functions. Ultimately, this free energy in the particle distribution functions is transferred to small scales in velocity space through an entropy cascade (Schekochihin et al. 2009; Tatsuno et al. 2009; Plunk et al. 2010; Plunk & Tatsuno 2011), enabling arbitrarily weak collisions to thermalize this energy, increasing the entropy and leading to irreversible heating of the plasma. Wave-particle interactions via the Landau resonance typically peak at $k_{\perp}\rho_i \sim 1$ for ions and $k_{\perp}\rho_i > 1$ for electrons, so the predicted result for ion-to-electron heating Q_i/Q_e is sensitive to the model for the nonlinear energy transfer rate in the kinetic Alfvén wave cascade.

Although the physical model of the turbulent cascade presented here remains controversial within the heliospheric physics community, there exists significant numerical and observational evidence in support of two of its key features: (1) the turbulent frequency remains low, $\omega \ll \Omega_i$, even for $k_{\perp}\rho_i \gtrsim 1$; and (2) the turbulence transitions to a cascade of kinetic Alfvén waves at $k_{\perp}\rho_i \sim 1$. A gyrokinetic numerical simulation of the transition from the MHD Alfvén wave to the kinetic Alfvén wave cascade at $k_{\perp}\rho_i \gtrsim 1$ (Howes et al. 2008b) produces magnetic and electric energy spectra that are consistent with *Cluster* measurements of turbulence in the solar wind (Bale et al. 2005). A recent gyrokinetic simulation spanning the entire dissipation range from the ion to the electron Larmor radius (Howes et al. 2011) yields a magnetic energy spectrum that is quantitatively consistent with *in situ* measurements of the dissipation range turbulence up to 100 Hz (Sahraoui et al. 2009; Kiyani et al. 2009; Alexandrova et al. 2009; Chen et al. 2010; Sahraoui et al. 2010). The striking agreement between the predictions for a kinetic Alfvén wave cascade and the observed magnetic and electric power spectra found by Sahraoui et al. (2009) provide observational support for this model. Finally, a k -filtering analysis of multi-spacecraft *Cluster* measurements demonstrates

that the wavevectors of the turbulent fluctuations at scales $k_{\perp}\rho_i \sim 1$ are aligned nearly perpendicular to the local magnetic field (Sahraoui et al. 2010); for Alfvénic turbulent fluctuations, this implies low turbulent frequencies, $\omega \ll \Omega_i$, in support of the turbulent model employed in this study.

2.3. Turbulent Heating Prediction

Assuming a fully ionized plasma of protons and electrons with isotropic Maxwellian equilibrium velocity distributions, Howes (2010) used the turbulent cascade model (Howes et al. 2008a) to calculate the total proton and electron heating resulting from collisionless damping of the electromagnetic fluctuations of the Alfvénic turbulent cascade. The model employs the linear collisionless gyrokinetic dispersion relation (Howes et al. 2006) to determine both the linear kinetic damping rate via the Landau resonances and the nonlinear energy cascade rate, so the resulting heating prescription is only valid in the gyrokinetic limit, $\omega \ll \Omega_p$.

The resulting prescription for the ratio of proton-to-electron heating for $T_p/T_e > 1$ is given by

$$Q_p/Q_e = c_1 \frac{c_2^2 + \beta_p^\alpha}{c_3^2 + \beta_p^\alpha} \sqrt{\frac{m_p T_p}{m_e T_e}} e^{-1/\beta_p} \quad (5)$$

where $c_1 = 0.92$, $c_2 = 1.6/(T_p/T_e)$, $c_3 = 18 + 5 \log(T_p/T_e)$, and $\alpha = 2 - 0.2 \log(T_p/T_e)$. The requirement that the proton cyclotron resonance plays a negligible role in the dynamics and dissipation of the turbulence enables the regime of validity of this turbulent heating prescription to be quantified. The limit of the regime of validity can be expressed as a constraint on the minimum width of the inertial range $(k_0\rho_p)^{-1}_{min}$, shown in panel (a) of Figure 2 as a contour plot in the $(\beta_p, T_p/T_e)$ parameter space.

Substituting the values of $\beta_p(R)$ and $T_p/T_e(R)$ specified in §2.1 into equation (5) enables the calculation of the predicted ratio of proton-to-electron turbulent heating $Q_p/Q_e(R)$ as a function of heliocentric radius. In Figure 1, we plot the predicted ratio of proton-to-total turbulent heating $Q_p/(Q_p + Q_e)$ vs. heliocentric radius R .

We compare this theoretical prediction to the the empirical estimate by Cranmer et al. (2009) (dashed) for $0.8 \text{ AU} \lesssim R \leq 5.4 \text{ AU}$ in Figure 1. The error estimates (dotted) in this figure are derived by attempting to account for the error arising from both modeling and observational uncertainties. Modeling uncertainties are derived by taking the curves for outflow speeds of 650, 700, 750, and 800 km s^{-1} in Figure 3(a) and colatitudes of 0, 15, and 30 degrees in Figure 4(b) of Cranmer et al. (2009). The observational uncertainties in the calculated turbulent heating due to observed variations in the proton and electron temperatures and electron heat flux are estimated roughly by taking $\pm 10\%$ of the proton-to-total turbulent heating ratio. The error estimates (dotted) plotted in Figure 1 are determined by taking the outer envelope of these modeling and observational uncertainties.

We find generally good agreement between the prediction of the turbulent heating prescription (solid) and the empirical estimate by Cranmer et al. (2009) (dashed) for $0.8 \text{ AU} \lesssim R \leq 5.4 \text{ AU}$. The disagreement at $R \lesssim 0.8 \text{ AU}$,

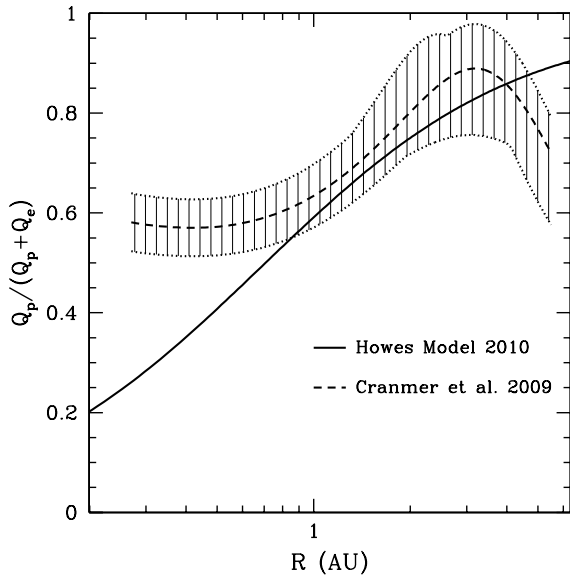


FIG. 1.— A comparison of the proton-to-total heating rate $Q_p/(Q_p + Q_e)$ as a function of heliocentric radius R : the solid line is the prediction based on the turbulent heating prescription given by equation (5) (Howes 2010), and the dashed line is the empirical estimate of Cranmer et al. (2009), where dotted lines indicate an error estimate to account for modeling and observational uncertainties.

as we shall see in §2.5, is attributed to the violation of the gyrokinetic approximation, and, therefore, to exceeding the limits of validity of the turbulent heating prescription. The downturn in the empirical estimate of $Q_p/(Q_p + Q_e)$ (dashed) seen at $R > 3$ AU may be an artifact of the bifurcation of the electron temperatures measured by *Ulysses*, as seen in Figure 1(a) of Cranmer et al. (2009), and may not represent an actual decrease in the proton-to-total turbulent heating ratio for the high-speed wind. Cranmer et al. (2009) noted that this appeared to be a solar cycle effect, but further work will be required to ascertain the significance of this downturn.

We can compare our prediction of the turbulent heating based on equation (5) with predictions based on simple theoretical models of the turbulent heating by Cranmer et al. (2009), presented in Figure 5 of their paper. Their approach used a quasilinear framework to estimate the proton-to-electron heating rates for three particular models of the distribution of turbulent energy in wavevector space: an isotropic distribution, a slab distribution of only parallel wavevectors, and a “two-dimensional” (2D) distribution of nearly perpendicular wavevectors. All three of the models showed significant disagreement with the empirically determined heating ratio. The slab model predicted 100% proton heating, the isotropic model overestimated the proton heating for $R \lesssim 2$ AU, and the 2D model significantly underestimated the proton heating at $R \gtrsim 1$ AU. In light of these results, the agreement between the proton-to-total turbulent heating ratio predicted by equation (5) and the empirical estimate in Figure 1 is quite good. This result suggests that the turbulent cascade model (Howes et al. 2008a) captures the dominant physical mechanisms (described qualitatively in §2.2) that play a role in the dissipation of solar wind turbulence at $\gtrsim 0.8$ AU.

The disagreement between the prediction of the

R (AU)	f_0 (HZ)	L_0 (km)	k_0 (rad km ⁻¹)
0.3	6×10^{-3}	1.2×10^5	5.2×10^{-5}
0.7	1.5×10^{-3}	4.7×10^5	1.3×10^{-5}
0.9	6×10^{-4}	1.2×10^6	5.2×10^{-6}

TABLE 1
MEASURED VALUES OF THE FREQUENCY f_0 OF THE OUTER SCALE OF THE INERTIAL RANGE OF SOLAR WIND TURBULENCE MEASURED BY *Helios 2*.

proton-to-total turbulent heating ratio (solid) and the empirical estimate (dashed) in Figure 1 can be understood if we evaluate the limit of the regime of validity of the turbulent heating prescription (eq. [5]) using the plasma parameters specified for the solar wind model in §2.1. The violation of the gyrokinetic approximation, or, equivalently, the point at which the proton cyclotron resonance begins to play a non-negligible role in the dynamics and dissipation of the turbulence, is cast as a requirement for the minimum dynamic range spanned by the inertial range, given by the driving scale divided by the proton Larmor radius, $L_0/\rho_p \sim (k_0\rho_p)^{-1}$. We denote this as the minimum “width” of the inertial range, $(k_0\rho_p)_{min}^{-1}$, plotted in panel (a) of Figure 2 as a contour plot in the $(\beta_p, T_p/T_e)$ parameter space. The proton Larmor radius $\rho_p = v_{tp}/\Omega_p = c(2T_p m_p)^{1/2}/(q_p B)$ is easily determined as a function of heliocentric distance R given the models for $T_p(R)$ and $B(R)$ given in §2.1. Estimating isotropic driving wavenumber of the turbulence $k_0(R)$, however, requires the incorporation of additional empirical constraints.

2.4. Evolution of the Width of the Inertial Range

We interpret the isotropic driving scale $L_0 = 2\pi/k_0$ to be the outer scale of the inertial range, and we identify this scale observationally as the break in the solar wind magnetic energy spectrum from the f^{-1} energy containing range to the $f^{-5/3}$ inertial range. To estimate k_0 , we employ measurements of magnetic energy spectrum from *Helios 2* data published in Figure 23 of Bruno & Carbone (2005). The frequency f_0 of the spectral break marking the outer scale of the inertial range measured from this figure is given in Table 1. Each of these spectra are measured in the same corotating fast stream with a velocity $v_{sw} \simeq 700$ km s⁻¹ (taken from Figure 17 of Bruno & Carbone (2005)), so we may calculate the corresponding inertial range outer scale length $L_0 = v_{sw}/f_0$, or wavenumber $k_0 = 2\pi/L_0$.

The function

$$k_0 = K_0 \left(\frac{R}{1 \text{ AU}} \right)^{-2} \quad (6)$$

provides a reasonable fit for the evolution of k_0 as a function of heliocentric radius R with the value $K_0 = 5 \times 10^{-6}$ rad/km. Although this fit is based solely on measurements in the inner heliosphere and may not be an accurate representation of the evolution of $k_0(R)$ for $R > 0.9$ AU, we will see that error in the estimation of k_0 at $R \gtrsim 1$ AU does not strongly impact the applicability of the turbulent heating prescription for the plasma parameters derived from this solar wind model.

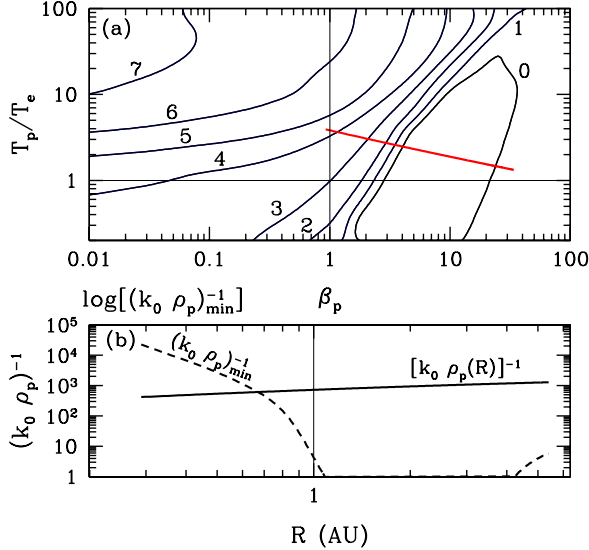


FIG. 2.— (a) Logarithmic contour plot of the minimum width of the inertial range $(k_0 \rho_p)^{-1}_{min}$ over the plane $(\beta_p, T_p/T_e)$, the condition required for the the proton cyclotron resonance to play a negligible role. The red line denotes the evolution plasma parameters of the solar wind model in §2.1 from $R = 0.29$ AU (left end) to $R = 5.4$ AU (right end). (b) The minimum width of the inertial range $(k_0 \rho_p)^{-1}_{min}$ along the red line in panel (a) (dashed) vs. the estimated width of the inertial range $(k_0 \rho_p)^{-1}$ for the solar wind model considered here (solid). For the heating prescription to be valid, the dashed line must fall below the solid line.

2.5. Evaluation of the Limits of Validity of the Turbulent Heating Prescription

Using the values of $\rho_p(R)$ and $k_0(R)$ derived here, we calculate the width of the inertial range $k_0 \rho_p$ as a function of heliocentric radius and compare it to the constraint on $(k_0 \rho_p)^{-1}_{min}$, as shown in Figure 2. Panel (a) presents a logarithmic contour plot of the constraint $(k_0 \rho_p)^{-1}_{min}$ over the $(\beta_p, T_p/T_e)$ parameter space. Also shown is the path through this parameter space (red) traversed by the solar wind model from 0.29 AU to 5.4 AU. In panel (b), the value of the width of the inertial range $(k_0 \rho_p)^{-1}$ for our solar wind model (solid) is plotted against the constraint on the minimum width of the inertial range $(k_0 \rho_p)^{-1}_{min}$ for the validity of our heating model (dashed). (For the heating prescription to be valid, the dashed line must fall below the solid line in this plot.) As previously mentioned, for the plasma parameters β_p and T_p/T_e specified by the solar wind model in §2.1, the constraint on $(k_0 \rho_p)^{-1}_{min}$ does not strongly restrict the applicability of the heating prescription for $R > 1$ AU. It is clear, however, that this constraint is violated for heliocentric distances $R \lesssim 0.7$ AU, signaling that the gyrokinetic representation of the turbulent dissipation mechanisms is no longer valid because the proton cyclotron resonance has begun to play a non-negligible role. Significantly, this limit to the validity of our prediction for the proton-to-total turbulent heating ratio coincides with the point where our prediction (solid) begins to fall significantly below the empirical estimate (dashed) in Figure 1. If the contribution to proton heating from the proton cyclotron resonance becomes non-negligible for heliocentric distances $R \lesssim 0.8$ AU, a physical pro-

cess not represented in the gyrokinetic turbulent heating prescription, then the result would be an empirically estimated proton-to-total heating rate that exceeds the gyrokinetic predictions at these radii, in agreement with the behavior shown in Figure 1.

3. DISCUSSION

The results presented in §2 suggest the following consistent picture of the physical mechanisms in the high-speed solar wind that are responsible for the dissipation of the turbulence and that lead to heating of the plasma protons and electrons.

In the inner heliosphere at $R \lesssim 0.8$ AU, the typically high T_p/T_e and low β_p conditions (coupled with a slightly smaller width of the inertial range $(k_0 \rho_p)^{-1}$; see panel (b) of Figure 2) in high-speed streams lead to a turbulent cascade in which the small scale turbulent fluctuations can reach the proton cyclotron frequency before the turbulence is collisionlessly damped via the Landau resonances. Therefore, one may expect to observe greater heating of the protons than that predicted by the turbulent heating prescription given by equation (5), a result based on a gyrokinetic cascade model (Howes et al. 2008a). By the time the turbulence has reached $R > 0.8$ AU, the decrease of T_p/T_e and increase of β_p (coupled with a slight increase in the width of the inertial range $(k_0 \rho_p)^{-1}$; see panel (b) of Figure 2), lead to plasma conditions in which the turbulent cascade no longer is affected by the proton cyclotron resonance before it is terminated by collisionless damping via the Landau resonances. Thus, for the range $0.8 \text{ AU} \lesssim R \leq 5.4 \text{ AU}$, the turbulent heating prescription in the gyrokinetic limit adequately represents all of the physical mechanisms needed to reproduce the empirically estimated proton-to-total turbulent heating ratio, as seen in Figure 1.

This theoretical prediction of non-negligible proton cyclotron damping within the inner heliosphere at $R \lesssim 0.8$ AU is consistent with observational evidence. Proton cyclotron damping is expected to lead to heating of the protons in the direction perpendicular to the local mean magnetic field (Lehe et al. 2009). In the absence of such perpendicular proton heating, double adiabatic evolution would lead to a constant value of $T_{\perp p}/B$ as a function of heliocentric radius (Chew et al. 1956). *Helios* observations demonstrate that the constancy of $T_{\perp p}/B$ is indeed violated within the inner heliosphere (Marsch et al. 1983).

It is important to note that the observed non-adiabatic $T_{\perp p}/B$ does not directly identify the physical mechanism responsible. In addition to heating via the proton cyclotron resonance, several other physical mechanisms could lead to the observed behavior, including stochastic proton heating and kinetic proton temperature anisotropy instabilities.

Stochastic heating had been proposed as a mechanism for perpendicular proton heating for some time (Johnson & Cheng 2001; Chen et al. 2001; White et al. 2002; Voitenko & Goossens 2004; Bourouaine et al. 2008), and recently Chandran et al. (2010) have put forth strong theoretical and numerical evidence for stochastic perpendicular heating of protons at low plasma β by kinetic Alfvén waves of sufficient amplitude. Chandran (2010) has used these results for stochastic

heating to explain proton and minor ion perpendicular temperature observations in coronal holes. For the low plasma β conditions found in the inner heliosphere, it is possible that this mechanism of stochastic heating could explain the perpendicular proton temperature measurements (Marsch et al. 1983) and the empirically estimated proton heating (Cranmer et al. 2009) at $R \lesssim 0.8$ AU.

In addition, kinetic proton temperature anisotropy instabilities in the spherically expanding solar wind flow have been shown to play a role in regulating the proton temperature anisotropy (Kasper et al. 2002; Hellinger et al. 2006; Bale et al. 2009). Although these instabilities cannot lead to a net heating of the proton species, they can mediate a transfer of energy from the parallel to the perpendicular temperature, and vice versa, and so may be a cause of the observed deviation from double adiabatic evolution of the perpendicular temperature of the protons (Marsch et al. 1983).

There are several possible limitations of the application of the turbulent heating prescription given by equation (5) to the problem of the heating due to the dissipation of solar wind turbulence. First, the model does not account for energy in compressible wave modes, such as the collisionless manifestation of the fast and slow MHD wave modes. If significant energy exists in these compressible modes, any heating due to the dissipation of these modes must be handled separately. Second, the cascade model is constructed specifically for the case of balanced Alfvén wave energy fluxes up and down the local magnetic field, corresponding to zero cross helicity. Observations of the cross helicity in the high-latitude wind typically show non-zero normalized cross helicities varying over the range $0.2 \leq \sigma_c \leq 0.6$ (Bavassano et al. 2000a,b). Note, however, that a cross helicity of $\sigma_c = 0.6$ corresponds to the amplitude of anti-sunward waves only a factor of 2 larger than the sunward waves. Since the typical energy cascade rates in strong MHD turbulence vary linearly with the wave amplitudes (Goldreich & Sridhar 1995; Howes et al. 2008a), this level of imbalance in the turbulence is unlikely to yield significant qualitative differences compared to the balanced case. Third, the simplifying assumption of a fully ionized proton and electron plasma with isotropic Maxwellian equilibrium velocity distributions neglects the physical variations that may arise from the more complicated equilibrium conditions often observed in the solar wind. Such conditions include temperature anisotropy with respect to the local magnetic field direction (often treated using a bi-Maxwellian equilibrium distribution), significant deviations from a Maxwellian distribution at high energy, and the presence of minor ions, particularly helium. Nonetheless, we believe that the results presented here represent a significant step forward in our understanding of the mechanisms responsible for proton and electron heating in the turbulent solar

wind. Future work will explore the implications of these additional effects if any of them appears to impact significantly the findings presented here.

4. CONCLUSIONS

In the effort to identify the physical mechanisms that govern the dissipation of solar wind turbulence and lead to heating of the solar wind protons and electrons, Cranmer et al. (2009) made a great stride forward by determining an empirical estimate of the proton-to-total plasma heating in the high-speed solar wind using *Helios* and *Ulysses* data. Based on a turbulent energy cascade model for low-frequency, anisotropic Alfvénic turbulence in a weakly collisional plasma (Howes et al. 2008a), Howes (2010) constructed an analytical prescription for the total proton-to-electron heating resulting from collisionless damping of the electromagnetic fluctuations of the Alfvénic turbulence.

Applying this turbulent heating prescription to predict the proton-to-total plasma heating in the high-speed solar wind, we obtain the following results, as shown in Figure 1: (1) the prediction agrees well with the empirical estimate for $0.8 \text{ AU} \lesssim R \leq 5.4 \text{ AU}$; (2) the predicted proton heating falls below the empirical estimate for $R \lesssim 0.8 \text{ AU}$. Investigating the cause of the disagreement for $R \lesssim 0.8 \text{ AU}$, we see, in panel (b) of Figure 2, that the turbulent heating prescription in the gyrokinetic limit ceases to be valid for $R \lesssim 0.7 \text{ AU}$. This failure of the prescription’s validity has physical meaning. In this region, the cascade model predicts that the turbulent fluctuations will reach the proton cyclotron frequency before they are damped via the Landau resonances. Therefore, we expect that proton cyclotron damping will cause additional proton heating, leading to an underestimate of the proton-to-total heating ratio, as seen in Figure 1.

These results suggest the following physical picture of the turbulent cascade and plasma heating in the high-speed solar wind. In the inner heliosphere at $R \lesssim 0.8 \text{ AU}$, the turbulent cascade can reach the proton cyclotron frequency, leading to a level of proton heating higher than that predicted by the turbulent heating prescription in the gyrokinetic limit. But for heliocentric radii $R \gtrsim 0.8 \text{ AU}$, collisionless damping via the Landau resonances terminates the turbulent cascade before the proton cyclotron resonance is reached, so the turbulent heating prescription in the gyrokinetic limit contains all of the necessary physical mechanisms needed to reproduce the empirically estimated proton-to-total heating ratio.

G. G. H. thanks Steve Cranmer for insightful discussions and for providing his empirical heating data with error estimates. The work has been supported by NSF CAREER Award AGS-1054061 and NASA NNX10AC91G.

REFERENCES

- Alexandrova, O., Saur, J., Lacombe, C., Mangeney, A., Mitchell, J., Schwartz, S. J., & Robert, P. 2009, *Phys. Rev. Lett.*, 103, 165003
- Bale, S. D., Kasper, J. C., Howes, G. G., Quataert, E., Salem, C., & Sundkvist, D. 2009, *Phys. Rev. Lett.*, 103, 211101
- Bale, S. D., Kellogg, P. J., Mozer, F. S., Horbury, T. S., & Reme, H. 2005, *Phys. Rev. Lett.*, 94, 215002
- Bavassano, B., Pietropaolo, E., & Bruno, R. 2000a, *J. Geophys. Res.*, 105, 12697
- . 2000b, *J. Geophys. Res.*, 105, 15959
- Boldyrev, S. 2005, *Astrophys. J. Lett.*, 626, L37
- Bourouaine, S., Marsch, E., & Vocks, C. 2008, *Astrophys. J. Lett.*, 684, L119

- Breech, B., Matthaeus, W. H., Cranmer, S. R., Kasper, J. C., & Oughton, S. 2009, *Journal of Geophysical Research (Space Physics)*, 114, 9103
- Breech, B., Matthaeus, W. H., Minnie, J., Bieber, J. W., Oughton, S., Smith, C. W., & Isenberg, P. A. 2008, *Journal of Geophysical Research (Space Physics)*, 113, 8105
- Bruno, R., & Carbone, V. 2005, *Living Reviews in Solar Physics*, 2, 4
- Chandran, B. D. G. 2010, *Astrophys. J.*, 720, 548
- Chandran, B. D. G., Li, B., Rogers, B. N., Quataert, E., & Germaschewski, K. 2010, *Astrophys. J.*, 720, 503
- Chen, C. H. K., Horbury, T. S., Schekochihin, A. A., Wicks, R. T., Alexandrova, O., & Mitchell, J. 2010, *Physical Review Letters*, 104, 255002
- Chen, L., Lin, Z., & White, R. 2001, *Phys. Plasmas*, 8, 4713
- Chew, G. L., Goldberger, M. L., & Low, F. E. 1956, "Proc. R. Soc. London A", 236, 112
- Cranmer, S. R., Matthaeus, W. H., Breech, B. A., & Kasper, J. C. 2009, *Astrophys. J.*, 702, 1604
- Frieman, E. A., & Chen, L. 1982, *Phys. Fluids*, 25, 502
- Goldreich, P., & Sridhar, S. 1995, *Astrophys. J.*, 438, 763
- Gruzinov, A. V. 1998, *Astrophys. J.*, 501, 787
- Hellinger, P., Trávníček, P., Kasper, J. C., & Lazarus, A. J. 2006, *Geophys. Res. Lett.*, 33, 9101
- Howes, G. G. 2008, *Phys. Plasmas*, 15, 055904
- . 2010, *Mon. Not. Roy. Astron. Soc.*, 409, L104
- Howes, G. G., Cowley, S. C., Dorland, W., Hammett, G. W., Quataert, E., & Schekochihin, A. A. 2006, *Astrophys. J.*, 651, 590
- . 2008a, *J. Geophys. Res.*, 113, A05103
- Howes, G. G., Dorland, W., Cowley, S. C., Hammett, G. W., Quataert, E., Schekochihin, A. A., & Tatsuno, T. 2008b, *Phys. Rev. Lett.*, 100, 065004
- Howes, G. G., TenBarge, J. M., Dorland, W., Quataert, E., Schekochihin, A. A., Numata, R., & Tatsuno, T. 2011, *Phys. Rev. Lett.*, submitted
- Johnson, J. R., & Cheng, C. Z. 2001, *Geophys. Res. Lett.*, 28, 4421
- Kasper, J. C., Lazarus, A. J., & Gary, S. P. 2002, *Geophys. Res. Lett.*, 29, 20
- Kiyani, K. H., Chapman, S. C., Khotyaintsev, Y. V., Dunlop, M. W., & Sahraoui, F. 2009, *Phys. Rev. Lett.*, 103, 075006
- Kolmogorov, A. N. 1941, *Dokl. Akad. Nauk SSSR*, 30, 9, english Translation: *Proc. Roy. Soc. London A*, 434, 9 (1991)
- Leamon, R. J., Smith, C. W., Ness, N. F., & Wong, H. K. 1999, *J. Geophys. Res.*, 104, 22331
- Lehe, R., Parrish, I. J., & Quataert, E. 2009, *Astrophys. J.*, 707, 404
- Marsch, E., Muehlhaeuser, K. H., Rosenbauer, H., & Schwenn, R. 1983, *J. Geophys. Res.*, 88, 2982
- Matthaeus, W. H., Zank, G. P., Smith, C. W., & Oughton, S. 1999, *Physical Review Letters*, 82, 3444
- Plunk, G. G., Cowley, S. C., Schekochihin, A. A., & Tatsuno, T. 2010, *Journal of Fluid Mechanics*, 664, 407
- Plunk, G. G., & Tatsuno, T. 2011, *Phys. Rev. Lett.*, 106, 165003
- Quataert, E. 1998, *Astrophys. J.*, 500, 978
- Quataert, E., & Gruzinov, A. 1999, *Astrophys. J.*, 520, 248
- Rutherford, P. H., & Frieman, E. A. 1968, *Phys. Fluids*, 11, 569
- Sahraoui, F., Goldstein, M. L., Belmont, G., Canu, P., & Rezeau, L. 2010, *Phys. Rev. Lett.*, 105, 131101
- Sahraoui, F., Goldstein, M. L., Robert, P., & Khotyaintsev, Y. V. 2009, *Phys. Rev. Lett.*, 102, 231102
- Schekochihin, A. A., Cowley, S. C., Dorland, W., Hammett, G. W., Howes, G. G., Quataert, E., & Tatsuno, T. 2009, *Astrophys. J. Supp.*, 182, 310
- Smith, C. W., Matthaeus, W. H., Zank, G. P., Ness, N. F., Oughton, S., & Richardson, J. D. 2001, *J. Geophys. Res.*, 106, 8253
- Stawarz, J. E., Smith, C. W., Vaquez, B. J., Forman, M. A., & MacBride, B. T. 2009, *Astrophys. J.*, 697, 1119
- Tatsuno, T., Schekochihin, A. A., Dorland, W., Plunk, G., Barnes, M. A., Cowley, S. C., & Howes, G. G. 2009, *Phys. Rev. Lett.*, 103, 015003
- Voitenko, Y., & Goossens, M. 2004, *Nonlinear Processes in Geophysics*, 11, 535
- White, R., Chen, L., & Lin, Z. 2002, *Phys. Plasmas*, 9, 1890
- Zank, G. P., Matthaeus, W. H., & Smith, C. W. 1996, *J. Geophys. Res.*, 101, 17093